

# Detection and Determination of Critical Phosphorus Source Areas Using Remote Sensing Data in Al-Abrash basin in Syria

## Hani Mohammad Ibraheem<sup>1\*</sup>, Younes Edriss<sup>2</sup> and Mohammad Said Al-Shater<sup>3</sup>

<sup>1</sup>Postgraduate Studies, Faculty of Agriculture, Soil Science, Damascus University, Syria

<sup>2</sup>General Organization of Remote Sensing, Damascus, Syria

<sup>3</sup>Faculty of Agriculture, Soil Science, Damascus University, Syria

Reveived: April 2020

**Abstract:** The critical phosphorus source areas (CPSAs) were determined by identifying and integrating both the transport factors of phosphorus (soil erosion, surface runoff, slope and Euclidean distance from water resources) and source factors (total phosphorus in the soil, land use and land cover) in Al-Abrash basin in Tartu's province, Syria during the winter season 2017-2018. The input data to the models, which were performed to determine the above mentioned six factors, consists of information through remote sensing, meteorological and soil data. The study indicated that CPSAs were located along Al-Abrash riverbanks. There are large areas of field crops and orchards in these regions, which relatively have high quantities of total phosphorus in the soils due to use of organic and inorganic fertilizers in previous stages and due to proximity of these agricultural areas to water resources (Al-Abrash river). In addition, CPSAs were located in the eastern part of Al-Abrash dam along the village of Beit Al-Sheikh Younis, and these regions are affected by high soil erosion due to various factors. The central and northern part of the study area was outside the water basin along the Smakah, Dananir, Ras Al Deir, Al-Awiya, Mashta Ghanem villages, which were planted by citrus and field crops. The study reflected that remote sensing data were basic for providing input for mathematical models so as to perform spatial analysis of CPSAs.

Key word: Phosphorus loss, soil erosion, runoff, land use, Al-Abrash basin.

The areas with high potential transport, which coincide with high P source areas on a landscape are considered as critical phosphorus source areas i.e. CPSAs (Sharpley and Jarvie, 2012; Xie and Zhao, 2016). Though many factors influence P loss, major factors have been taken into consideration based on previous studies such as surface runoff, precipitation, topography, soil erosion, euclidean distance from surface water, land use and land cover type and P concentration in soil. The surface runoff and soil inter flow can be generated with precipitation, and this process can significantly increase dissolved P loss (Chang, 2010; Liu et al., 2014). The surface runoff and soil erosion increases with slopes, and this also increases the dissolved P and particulate P loss (Hahn et al., 2014). The soil erosion is a complex process due to many parameters and it directly increases particulate P loss (Butler et al., 2006; Kahiluoto et al., 2015). As results of land use and land cover changes, which are driven by human activity, the increase in agricultural land leads to more and more

fertilizer use, and this results in accumulation of high levels of P in the soil and consequently more P loss occurs (McDowell, 2012; Lou et al., 2015). The concentration of P in agricultural land is increasing globally, which leads to accumulation of high levels of P in the surface soil and also its loss to water sources (Withers et al., 2014). Factors that drive the increase in CPSAs can be classified into two groups: P source factors (S factors), which include land use and land cover type and P concentration; and P transport factors (T factors) which include surface runoff, slope, euclidean distance from surface water and soil erosion. These factors were first determined by P loss researches using in situ experiments. The methods, which are used in detecting CPSAs, can be classified into three groups: isotope tracer technique, P-index models and eco hydrological models. Isotope trace technique uses radioactive elements to trace a P loss path and then determine the CPSAs (Wang et al., 2011a, 2011b). P-index model integrates transport and source factors to show vulnerability of area to the P loss, and thus to detect and determine CPSAs (Zhou and

\*E-mail: hani197865@yahoo.com

Gao, 2011). Eco-hydrological models are used to determine the CPSAs and these models are performed using remote sensing data (Rivero et al., 2009; Hahn et al., 2014). Isotope trace technique and the P index model generally concentrate on a big spatial scale. The isotope trace technique is more appropriate at plot scale (Wang et al., 2011a, 2011b), and P-index models have good performance at field scale, and farm scale (Zhou and Gao, 2011). Ecohydrological models are used at watershed scale (Ghebremichael et al., 2013), but it cannot account for all the major factors responsible for the increase in CPSAs. Remote sensing data can give us spatially and temporally accurate information, and results from remote sensing models can realize the discretization of P concentration and describe the pathway of P loss (Oyama et al., 2015; Shi et al., 2016). The present study aims to: 1) detect CPSAs at a regional scale by incorporating remote sensing data with six driving factors and 2) display the spatial distribution of the CPSAs and their extent at the study area.

## Study Area

This study was conducted in Al-Abrash basin. It is geographically located in the south of Tartus province, located in the north west of Syria. The study area lies between longitudes (35.94135° and 36.18017°) east and latitudes (34.84333° and 34.653851°) north and covers 285 km² area bordered on the west by the Mediterranean Sea (Fig. 1). The landform of the study area is characterized by very complicated mountain systems and the elevation increases from west to east ranged from 4 to 400 m. The climate of the coastal area has good humidity

conditions, mild winter and warm rainless summer. The amount of the rainfall increases with altitude in the region that may reach to 1000 mm annually. Besides, the natural vegetation cover that mainly consists of various forest species like pine, cedar, fir, and oak one may also find olive groves, citrus orchards, various crops, and protected plantations.

### Materials and Methods

Data for CPSAs detection

The input data to the model consists of remote sensing data, meteorological and soil data. The remote sensing data included Digital Elevation Model DEM (30 m spatial resolution), Sentinel\_2 satellite image (10 m spatial resolution), which were obtained from free public data sources (http://earthexplorer. usgs.gov), and high spatial resolution satellite image from Google Earth platform. The meteorological data included precipitation from the Climate Hazards Group Infrared Precipitation with the Station data (CHIRPS) global monthly average rainfall with 5 km spatial resolution. The surface soil samples (151 soil samples) were collected randomly from the study area according to the land use/ land cover types and topographic properties to determine the total phosphorus (TP) in the soils. Sampling depth was (0-30 cm), and the position of each sampling loci was recorded by Global Position System (GPS).

Identification of the CPSAs at regional scale

The transport (T) factors (soil erosion, surface runoff, slope, Euclidean distance from surface water) and source (S) factors (total phosphorus

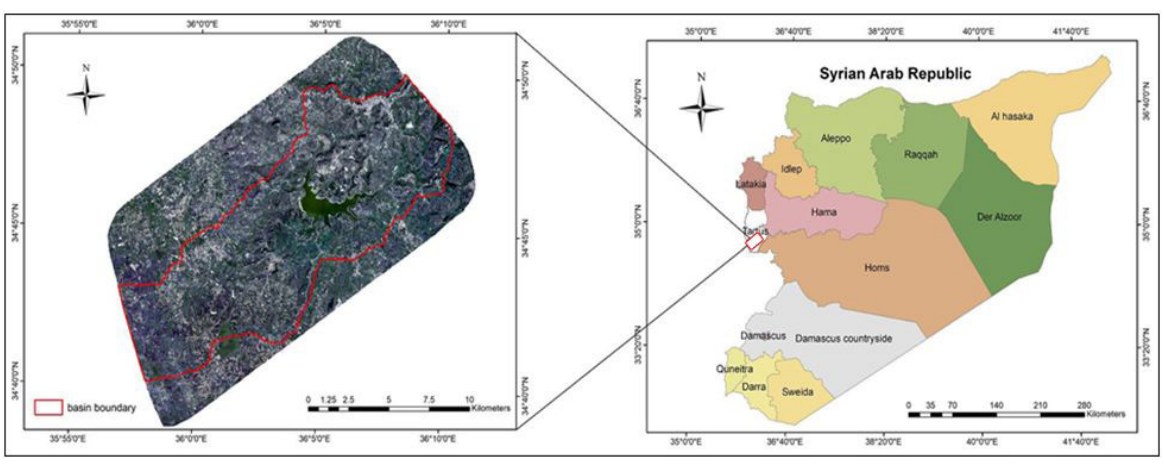


Fig. 1. Study area.

concentration (TP) in soil, land use and land cover) are integrated to locate the CPSAs at basin scale. The amount of soil erosion in the basin were calculated by the remote sensing driven Revised Universal Soil Loss Equation (RUSLE) (Wischmeier and Smith, 1978; Renard et al., 1991).

### A=R\*K\*LS\*C\*P

wherein, A represents average annual soil loss per unit area (t ha<sup>-1</sup> yr<sup>-1</sup>), R is rainfall erosivity factor (MJ mm ha<sup>-1</sup> h<sup>-1</sup> yr<sup>-1</sup>), K is soil erodibility factor (t ha h MJ<sup>-1</sup> ha<sup>-1</sup> mm<sup>-1</sup>), L is slope length factor, S is slope steepness factor, C is cover management factor, and P stands for support and conservation practices factor.

The depth of surface runoff was performed by rainfall-runoff modeling using the soil conservation service curve number (SCS-CN) model (SCS, 1985). The SCS-CN model is a well-established method in hydrology and environmental impact analysis and has been very popular because of its convenience, simplicity, and its responsiveness to four readily monitorable watershed properties (soil texture, land use/land cover, surface condition, and antecedent moisture condition; Ponce and Hawkins, 1996). The standard equations of the SCS – CN model is

$$Q = \frac{\left(P - I_a\right)^2}{P - I_a + S} \quad for \, I_a \le P, otherwise \, \, Q = 0$$

$$I_a = \lambda * S \text{ where } S = \frac{25400}{CN} - 254$$

P is total rainfall,  $I_a$  is initial abstraction, Q is direct runoff, S is potential maximum retention which can range  $(0, \infty)$ ,  $\lambda$  is initial abstraction coefficient or ratio, and CN (curve number) is empirical parameters, which are used to predict the direct runoff. It ranges from (0 to 100).

Slope is one of the most important measures of landscape characteristics, and it refers to the angle of inclination of a land surface above the horizontal, and can be calculated by geographic information systems through many mathematical equations (Chang and Tsai, 1991; Peucker and Douglas, 1974). Slope has been calculated using Digital Elevation Model (DEM) based on Shuttle radar topography mission (SRTM), at spatial resolution of 30 m. Euclidean distance from surface water in the basin was calculated in ArcGIS. The land use and land cover map of the basin was prepared

using rectified high spatial resolution satellite images from Google Earth and moderate spatial resolution satellite image Sentinel\_2 acquired on 8.9.2017 and using visual interpretation technique. The land use and land cover map was classified according to Syrian land use and land cover classification system and the area of each class was calculated per square kilometer. Multiple linear regression (MLR) by stepwise method was used to predict TP as dependent variable at locations from soil samples were not taken during the fieldwork. Soil properties (soil organic matter, sand, clay, silt, percentage total calcium carbonate, pH, electrical conductivity, bulk density) were used as independent variables. In addition, the spectral bands of satellite images (Bands 2, 3, 4, and 8 for Sentinel\_2 image), vegetation indices (Normalized Differences Vegetation Index (NDVI), Soil Adjusted Vegetation Index (SAVI), the Enhanced Vegetation Index (EVI), Modified Soil Adjusted Vegetation Index (MSAVI<sub>2</sub>), Optimized Soil Adjusted Vegetation Index (OSAVI), Transformed Vegetation Index (TVI), Ratio Vegetation Index (RVI), Green Ratio Vegetation Index (GRVI)) and topographic indices (slope, aspect) were used as auxiliary variables (independent variables) to predict TP using multiple linear regression equation. Selection of the factors to be included in the model was based on the Statistical tests (Freund and Littell, 2000). Figure 2 shows the spatial distribution of the soil samples in the study area. Here 100-point soil samples were used as training points to perform models for predicting the spatial distribution of TP at locations in which soil samples were not taken during the fieldwork, and 51-point soil samples as testing points to validate the results of those models. The model employed was described here under.

 $Y=a+b_1X_1+b_2X_2+b_nX_n+\varepsilon$ 

where Y represents predicted (TP) (dependent variable),  $(X_1, X_2, X_n)$  are variables which are affected by amount of TP in the soil (independent variables), 'a' is an intercept (constant),  $(b_1, b_2, b_n)$  are coefficients of the variables, ' $\epsilon$ ' are residuals (error).

The goodness of fit of the model was based on R<sup>2</sup> and probability levels. The stepwise regression analysis was used to select significant variables, by either accepting or eliminating the

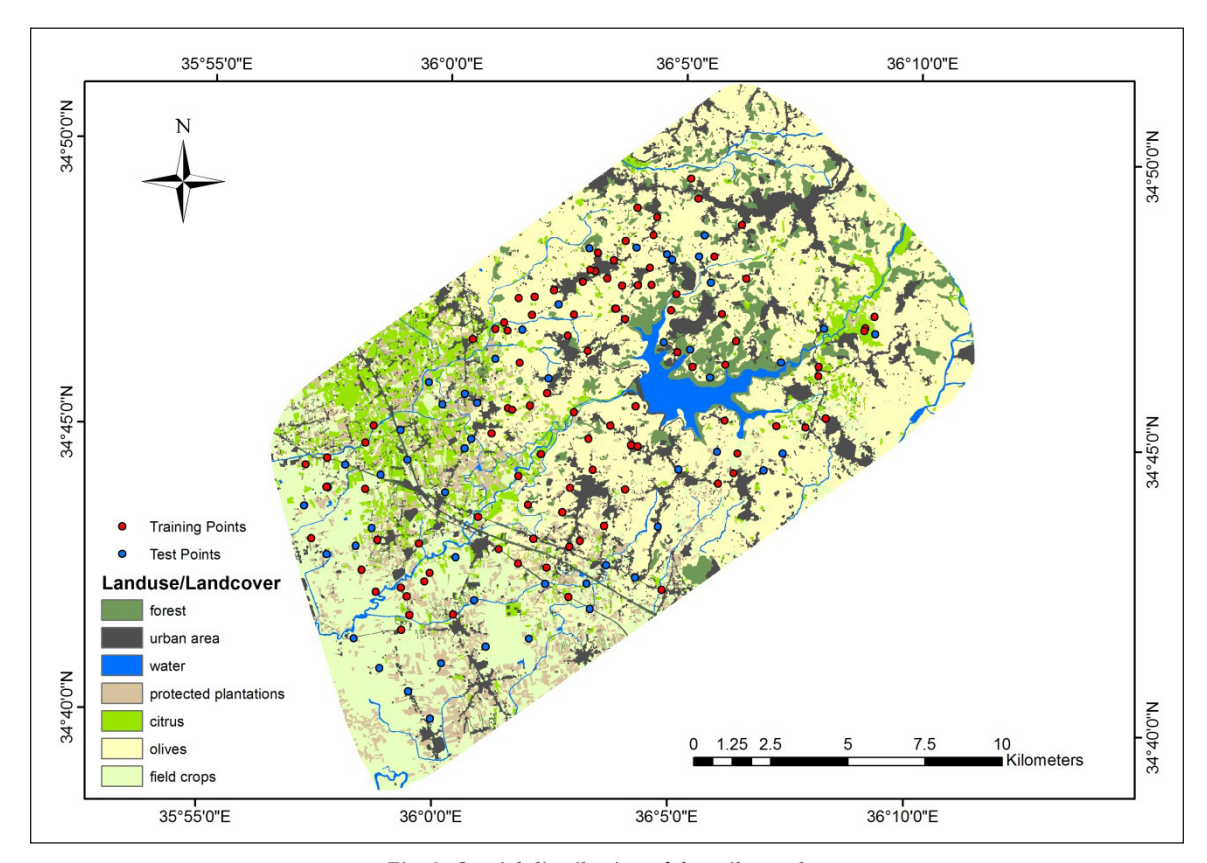


Fig. 2. Spatial distribution of the soil samples.

respective predictor variables, based on the significance of T-test.

Linear normalization method was used (Lou *et al.*, 2016) to export the values of the transport factors data, which are as previously mentioned (soil erosion, surface runoff, slope, euclidean distance from surface water) and source factors data (total phosphorus concentration

Table 1. Linear normalization method

CPSAS	Factors	Linear normalization method		
T factors	Soil erosion	$Y=0.1 + \frac{X-Min}{Max-Min}*(0.9-0.1)$		
	Surface runoff	$Y=0.1 + \frac{X-Min}{Max-Min}*(0.9-0.1)$		
	Slope	$Y=0.1 + \frac{X-Min}{Max-Min}*(0.9-0.1)$		
	Euclidean distance	$Y=0.1 + \frac{X-Min}{Max-Min}*(0.9-0.1)$		
S factors	Total phosphorus concentration	$Y=0.1 + \frac{X-Min}{Max-Min}*(0.9-0.1)$		
	land use and land cover	Olives=0.3, Citrus=0.4, Crops = 0.5, Forest = 0.1		

(TP) in soil, land use and land cover) to new values. Values ranged between (0.1 and 0.9) to facilitate comparison and analysis between the different variables, and to avoid the presence of abnormal maximum values during spatial analysis as shown in Table 1.

Weighting was assigned for each of the values (soil erosion, surface runoff, slope, euclidean distance, total phosphorus concentration (TP) in soil, land use and land cover) using ranking method (Roszkowska, 2013) according to effect of each of them on the fragile agriculture areas, and exposed to phosphorus loss. This means that the factors of the transport and the sources of the phosphorus were arranged from the most important to the least important in reference to the phosphorus loss in the study area. The rank sum method was chosen during the weighting process, which was carried out using the following formula (Roszkowska, 2013):

$$W_i = (n-r_j+1)/\sum (n-r_k+1)$$

where,  $W_i$  Adjusted weighting for j factor, n number of the factors under consideration (k=1, 2, 3....n),  $r_i$  rank position of the factor. Each

Raw	Factors	Rank	Weighting (n-r <sub>j</sub> +1)	Adjusted weighting
1	Soil erosion	1	6	0.286
2	Surface runoff	2	5	0.238
3	Slope	6	1	0.048
4	Euclidean distance	5	2	0.095
5	Total phosphorus concentration	3	4	0.19
6	Land use and land cover	4	3	0.143
	Sum		21	1

Table 2. Weights assigned to each factor based on the rank sum method

factor is weighted (n- $r_j$ +1) and then normalized by the sum of all weights  $\{\sum (n-r_k+1)\}$ . Table 2 shows the weights assigned to evaluate data layers.

The transport factors and source factors were integrated to locate the CPSAs at basin scale according to weighting values given in Table 2 and using Overlay weighted sum method in ArcGIS, as shown by the following equation.

$$CPSA_S = (ER*W_1) + (RU*W_2) + (TP*W_3) + (LU*W_4) + (D*W_5) + (S*W_6)$$

where, ER is soil erosion factor, RU is surface runoff, TP is total phosphorus in soil, LU is land use and land cover, D is euclidean distance, S is slope,  $W_1$  to  $W_6$  are weighting values.

The resulting map was then classified into five levels of severity of the phosphorus loss in the study area using Quartile classification method, which is considered an appropriate method for linearly distributed data. Figure 3 shows flowchart of the methodology adopted for the study.

### Results and Discussion

The quantity of soil erosion were classified into four classes according (Table 3) to the severity of the erosion (Mazahreh *et al.*, 2018).

It is clear from the Table 3 that about 38.5% of the study area not affected by soil erosion.

Table 3. Soil erosion classes and the percentage of the area under each soil erosion class

Area (%)	Soil loss rate (t ha <sup>-1</sup> year <sup>-1</sup> )	Intensity of erosion
38.5	0	No erosion
43.34	0-10	Low
1.4	10-50	Medium
0.07	50-200	High
0	> 200	Very high

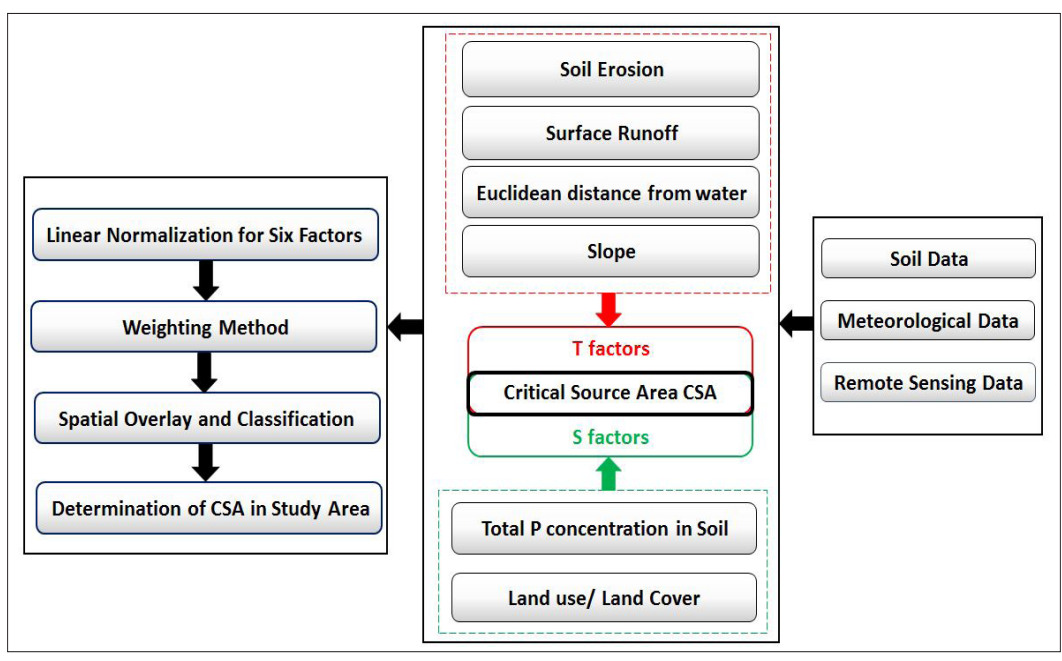
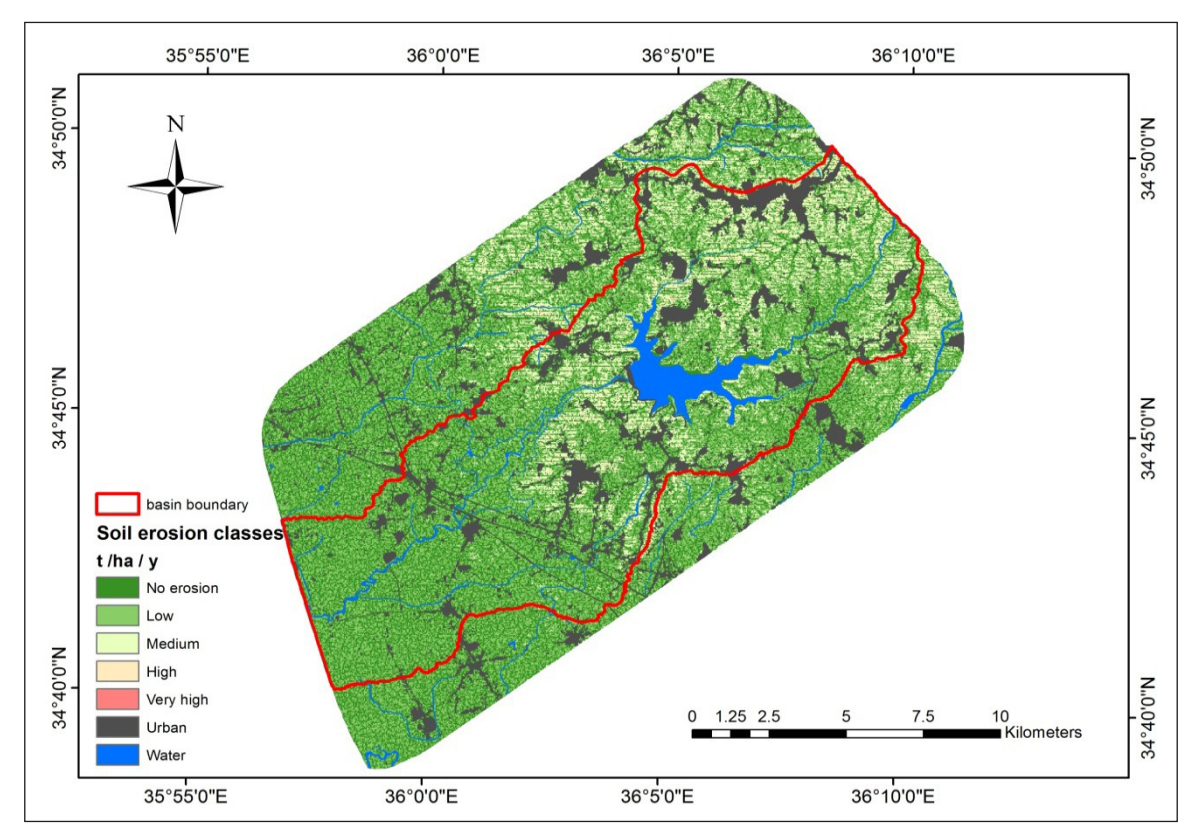


Fig. 3. Flow chart of the methodology.



 $Fig.\ 4.\ Spatial\ distribution\ of\ soil\ erosion\ classes.$ 

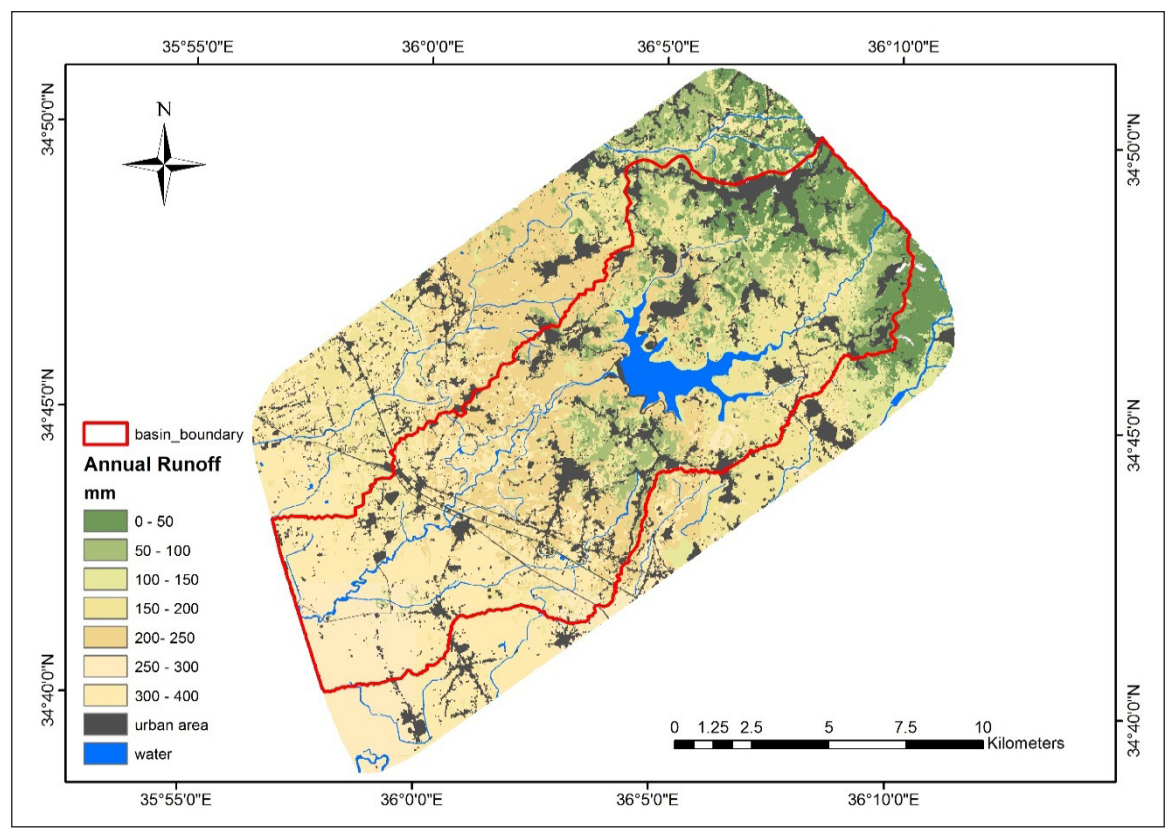


Fig. 5. Depth of annual runoff.

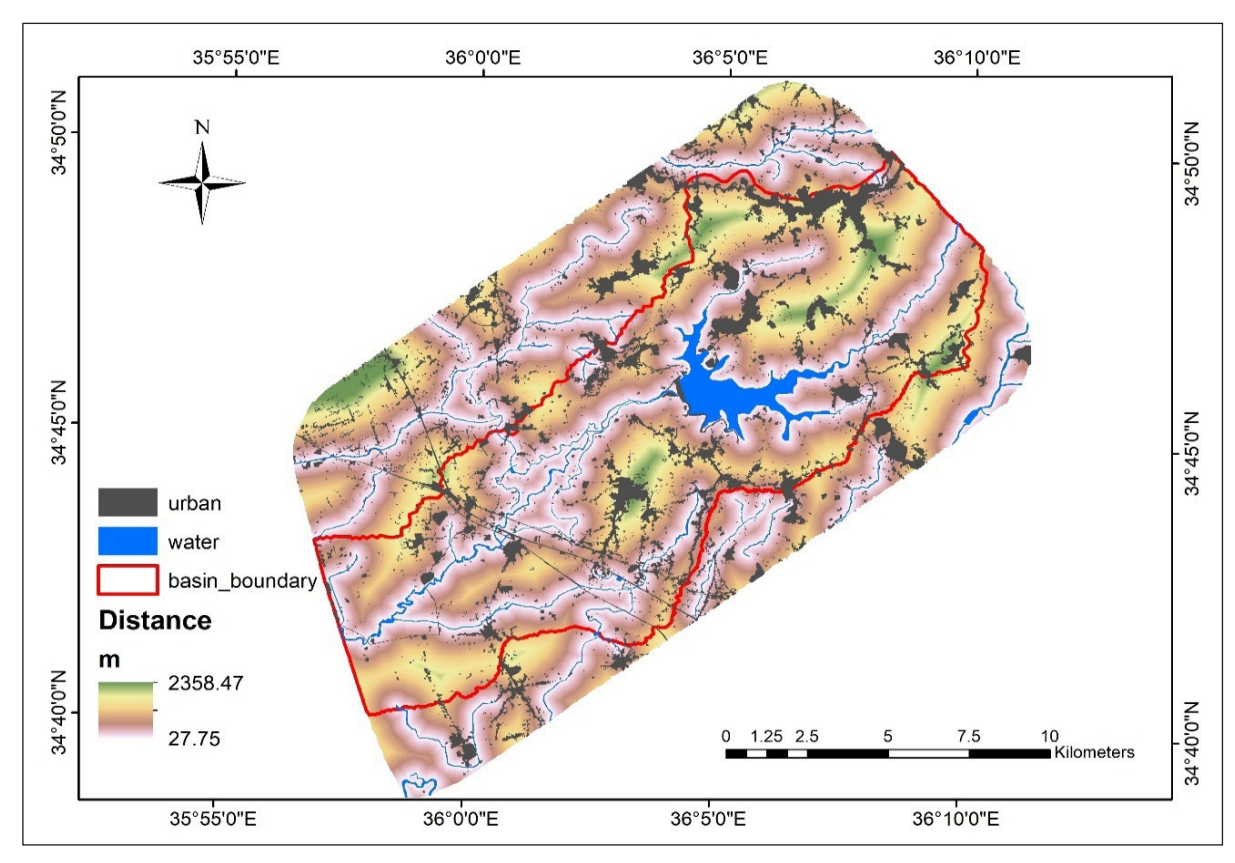


Fig. 6. Euclidean distance from surface water.

The low severity class represented about 43.34% of the total area, with a rate of soil loss less than (10 t ha<sup>-1</sup> y<sup>-1</sup>) and medium severity class constituted about 1.4% of the total area, with a rate of soil loss between (10-50 t ha-1 y-1). These results are consistent with the results obtained by Al-Abed et al., 2018. High values of soil erosion are observed mainly in the eastern and northeastern part of the study area (Fig. 4) due to integrated impacts of factors including the steep slopes, high precipitation, and soils with low depth located on limestone. While the western part of the study area was not affected by soil erosion as results of a combination of different factors, like flat land with low slope and deep clay loam, clay soils.

The amounts of runoff depth were classified to seven classes. Figure 5 represents the spatial distribution of the surface runoff depth classes in the study area for the period beginning October 2017 until May 2018 (Ibraheem *et al.*, 2019). The amounts of runoff were high in the western and southwestern part of the study area, and this may be due to the heavy soil texture (clay, clay loam), which does not allow

high permeability. Additionally, the cultivation of field crops does not prevent the surface runoff as observed in forests and orchards. In the eastern part of the study area the runoff depth decreased compared with the western part, and this may be due to soil texture (sandy loam, sandy clay loam) in the eastern parts, in addition to vegetation cover (forest, olive groves) which prevent the surface runoff significantly.

Figure 6 represents the spatial distribution of the euclidean distance from surface water in the study area, where the euclidean distance output grid, contains the measured distance from every cell in the study area to the nearest water resource and this ranged from 27.75 to 2358.47 m.

Spatial distribution of the degree slope in the study area (Fig. 7), was calculated using the (DEM) and Soil and Terrain Digital Database (SOTER) (Dobos *et al.*, 2007) wherein the classification of the slope as depicted in Table 4 was considered.

Distribution of land use and land cover classes in the study area reflected seven classes

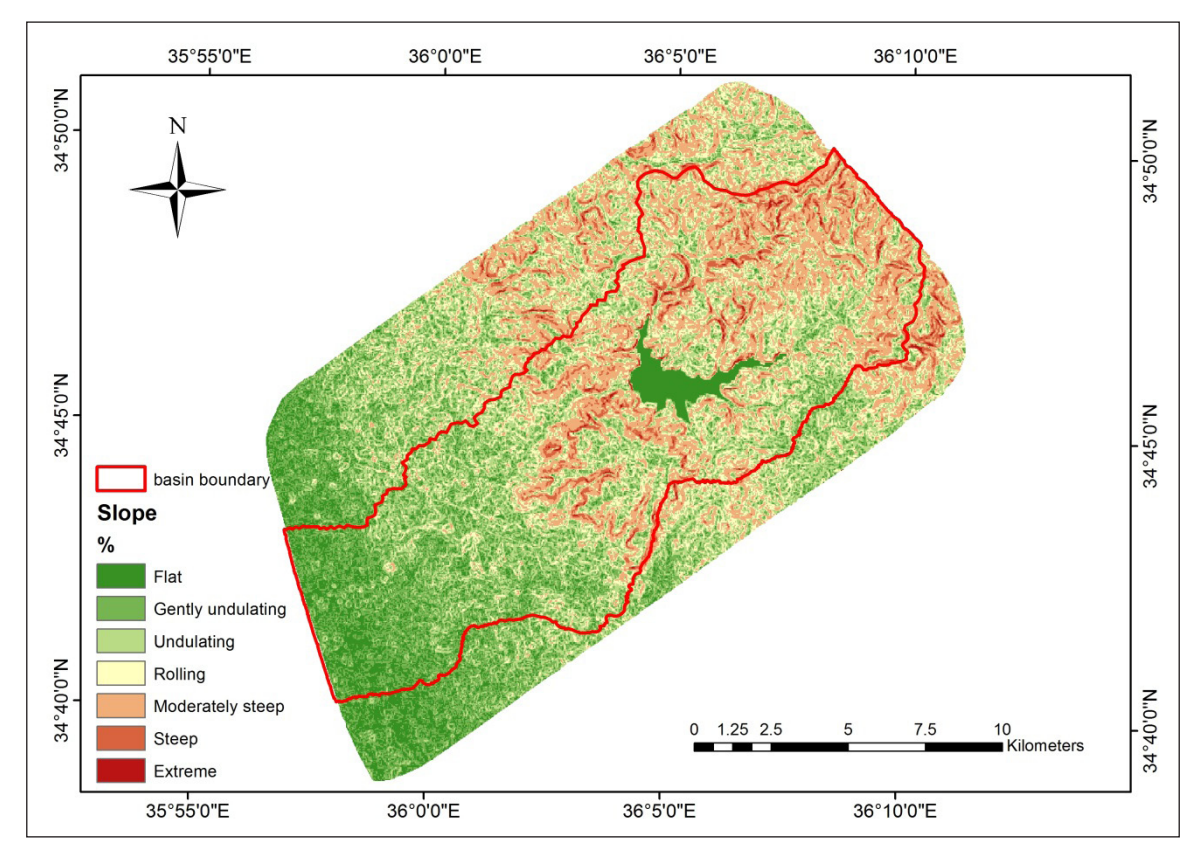


Fig. 7. Degree of the slope.

Table 4. The slope percentage and classes of topography

Topography	Slope percentage		
Flat	0-2		
Gently undulating	2-5		
Undulating	5-10		
Rolling	10-15		
Moderately steep	15-30		
Steep	30-45		
Extreme	Above 45		

(forest, urban, water, protected plantation, citrus orchards, olive groves, and field crops). Figure 8 shows the area of each class, where the olive groves class was 113.32 km², the citrus orchard 21.62 km², the forest area 17.81 km², field crops with protected plantation 83.93 km², urban area 37.67 km², and water area was 10.6 km².

From the results of the stepwise regression analysis, the equation for predicting the (TP)

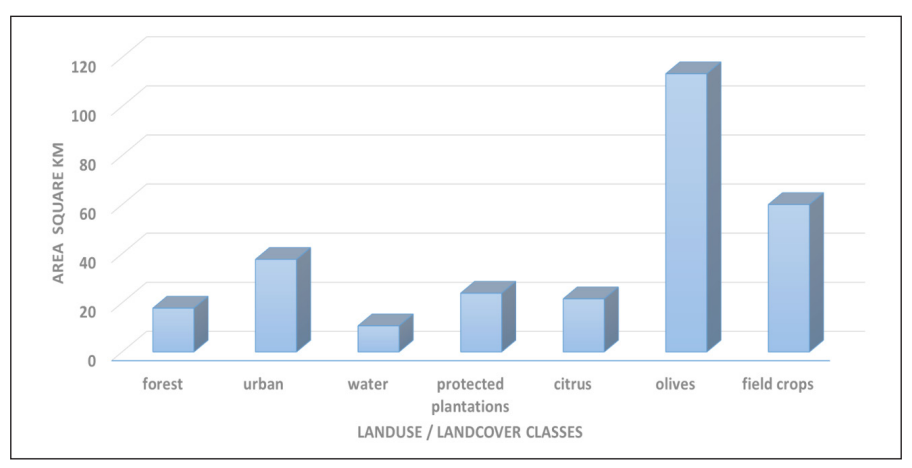


Fig. 8. Area of land use-land cover classes.

11	0 , 1 ,		
Land use and land cover	Upper values (mg kg-1)	Lower values (mg kg-1)	Average values (mg kg-1)
Forest	496.71	165.97	359.18
Citrus	494.31	173.71	390.68
Olives	473.17	145.59	324.83
Field crops	480.91	146.36	344.16

Table 5. Upper, lower and average values of total phosphorus

was established and applied in the study area. The values of total phosphorus in the soil ranged between 145.59 and 496.71 mg kg<sup>-1</sup>. Table 5 shows the upper, lower, average values of total phosphorus according to each class of land use and land cover classes in the study area.

High levels of (TP) were accumulated in the western and northwestern parts of the study area, which were planted by citrus and crops and have high quantities of total phosphorus in the soils due to use of organic and inorganic fertilizers in previous years, and also along Al-Abrash river banks from the eastern and western sides of the dam, where there are different crops (protected plantation, crops, and citrus). Figure 9 shows the spatial distribution of the total phosphorus in the study area.

The study demonstrated that the critical phosphorus source areas (CPSAs) were

established along Al-Abrash river banks before the dam along Al-Madafa to Al-Sisniyyah villages to Al-Abrash dam. Large areas of crops and orchards are located in these regions with high levels of (TP) in the soils. The intensive use of organic and inorganic fertilizers and proximity of these agricultural areas to water sources (Al-Abrash river) and canals leads to CPSAs. The CPSAs were also located before Al-Abrash dam, almost parallel to the previous villages along the village of Beit Al-Sheikh Younis to the village of Al-Mdeirjat until the dam. Figure 10 represents the spatial distribution of the villages along Al-Abrash river and around the dam. Further, these villages are affected by high soil erosion due to various factors.

The results are similar to findings of Al-Qutaini (2015) which indicated the presence of high turbidity in water samples in Al-Abrash dam during February after the rainy season,

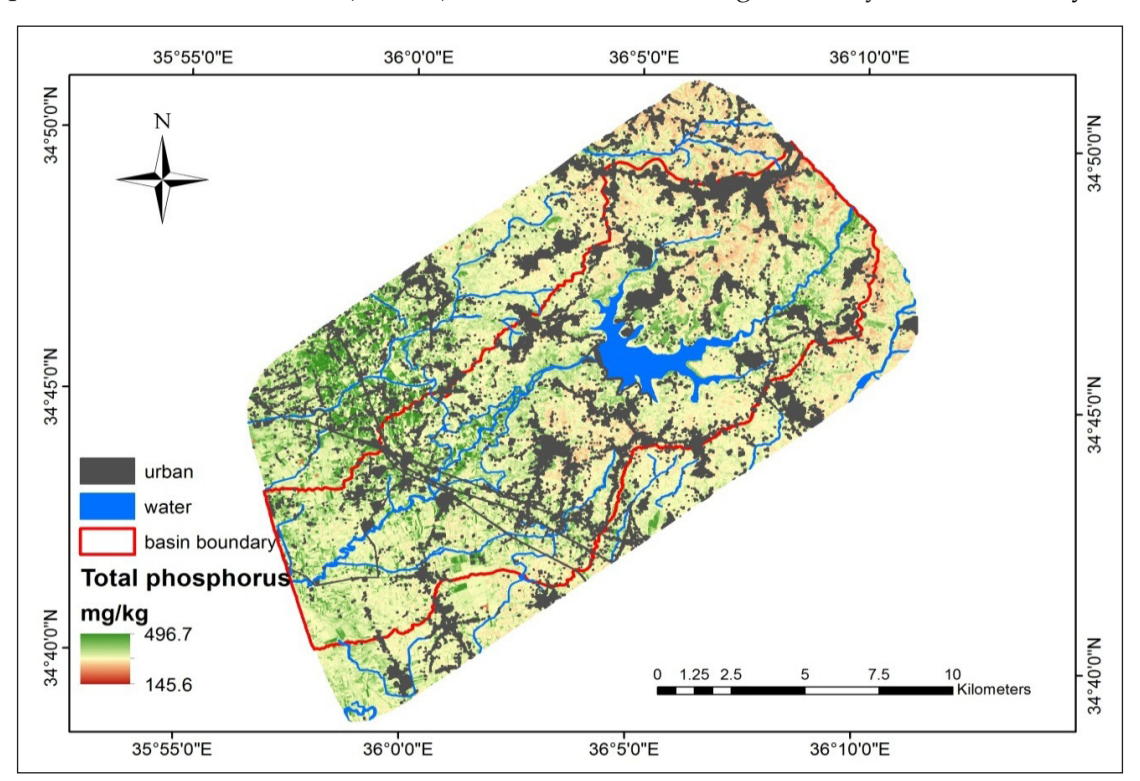


Fig. 9. Total phosphorus in soils.

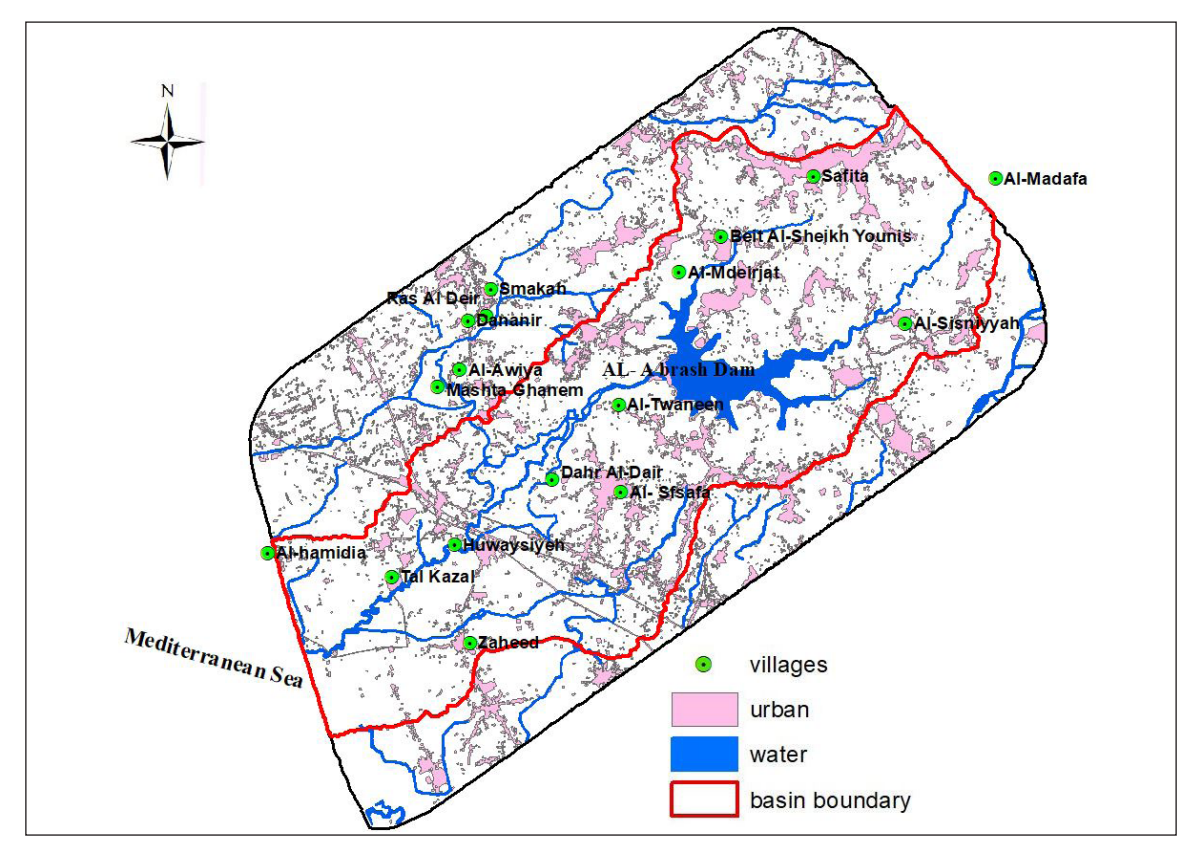


Fig. 10. Spatial distribution of the villages.

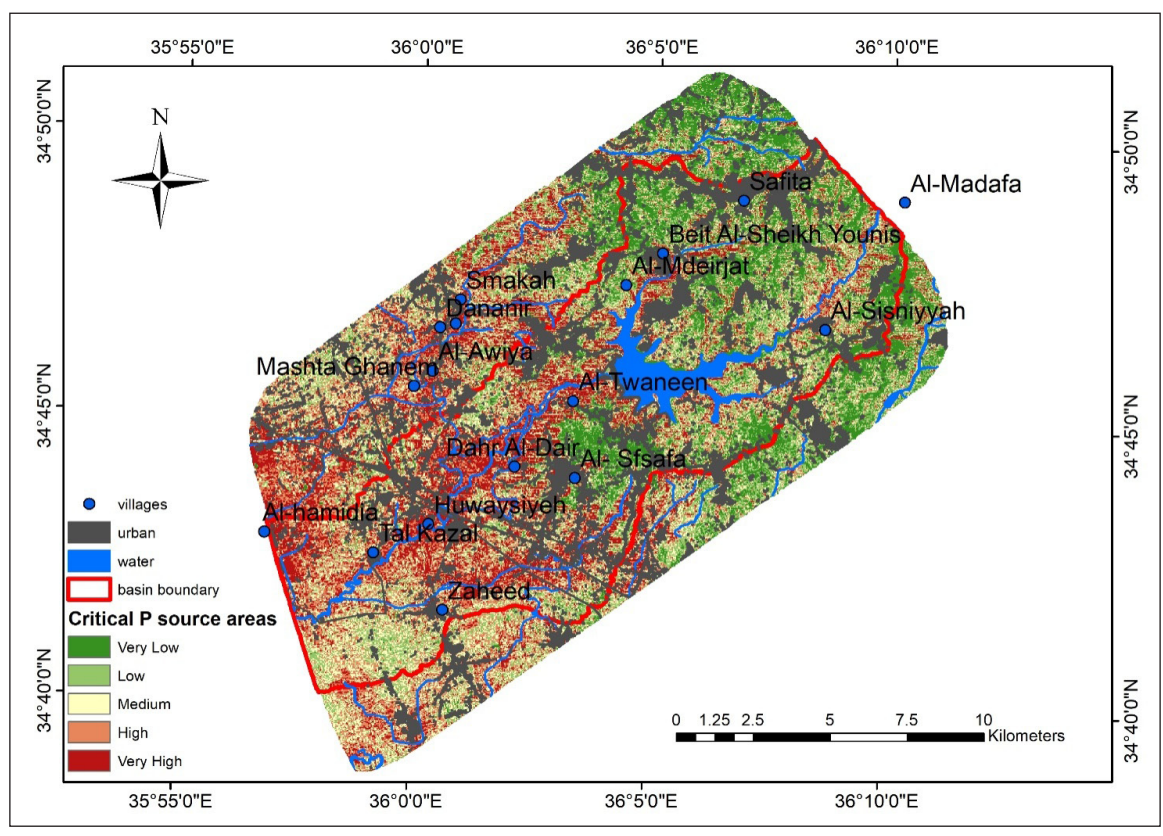


Fig. 11. Critical phosphorus source areas.

Land use/land cover	Phosphorus loss severity classes				
Vegetation type	Very low	Low	Medium	High	Very high
Forest	27.38	27.58	15.83	12.92	16.28
Olives	32.79	25.56	16.99	11.79	12.87
Citrus	4.86	20.06	29.28	28.24	17.55
Field crops	1.98	11.41	23.20	31.86	31.56

Table 6. Percentage of the area of different vegetation type under each different phosphorus loss severity classes

and also consistent with those reported by Yaghi and Salim (2017), where they showed the potential pollution areas with chemical fertilizers in Al-Abrash basin. The western part of the study area after Al-Abrash dam along Al-Twaneen, Dahr Al-Dair, Huwaysiyeh, Tal Kazal villages to the sea, which are exposed to high intensity of surface runoff due to a large amount of precipitation during winter, and heavy texture of the soil (clay, clay loam), was considered as CPSAs. CPSAs were located in the central and northern part of the study area outside the basin boundary along the villages Smakah, Dananir, Ras Al Deir, Al-Awiya, Mashta Ghanem. These areas were planted with citrus and field crops, and being closer to a network of rivers and canals are also exposed to soil erosion of medium intensity. Al-hamidia region, which is located to the west of the study area and close to the sea, were considered as CPSAs. These results are consistent with Al-Qutaini (2015), where the study showed a very high level of environmental pollution in the lower basin of Al-Abrash river, especially in Al-Sfsafa and Al-hamidia regions.

The pollution of Al-Abrash river with nitrogen and phosphorus compounds resulted in growth of aquatic plants in the river channel, which hindered the flow of water and threatened the aquatic life. Figure 11 represents the spatial distribution of the critical phosphorus source areas (CPSAs).

The percentage of the area of each critical phosphorus source areas in CPSAs of very low, low, medium, high, very high categories according to land use and land cover classes (forest, olives, citrus, field crops) in the study area (Table 6) revealed that low and very low severity class of phosphorus loss in the study area constituted about 54.96% and 58.35% of the total area of the forest and olives class, respectively. The average severity class represented about 15.83% and 16.99% of the total area for each of the forest and olives,

respectively. The high and very high severity class for phosphorus loss represented about 29.2% and 24.66% of the forest and olive class respectively. This indicates that more than half of the area of forest and olive class do not suffer from high risk of phosphorus loss, due to the interplay of different factors (total phosphorus, surface runoff, soil erosion). Relatively low total phosphorus concentrations in the soils of these two classes were observed compared to soils for both citrus and field crops. The low and very low risk classes of phosphorus loss were about 24.9% and 13.39% of the total area of each citrus and field crops class respectively. While the average severity classes represented about 29.28% and 23.2%, and the high and very high severity class for phosphorus loss was about 45.79% and 63.42% of the total area for both citrus and field crops respectively. This means that more than half areas of field crops and close to half area of the citrus class were considered as risk areas for phosphorus loss towards the water bodies due to high concentration of total phosphorus in the soils of these regions. This is probably due to use of high levels of fertilizers to achieve high agricultural production, especially in the western part of the study area, and also due to high intensity of surface runoff, which transports phosphorus to closer water bodies.

## Conclusion

The critical phosphorus source areas (CPSAs) were located along Al-Abrash riverbanks before and after Al-Abrash dam at the eastern and western parts of the study area. Various crops and citrus orchards are planted here which requires a large amount of phosphorus fertilization. The high and very high severity class for phosphorus loss was about 45.79% and 63.42% of the total area for citrus and field crops classes, respectively. In addition, the high and very high severity class for phosphorus loss was 29.2% and 28.78% of the forest and olive classes respectively. The

study showed the importance of the integration of transport and source factors of phosphorus for identifying and demarcating the critical phosphorus source areas. The study also demonstrated and demonstrated the important role of remote sensing data as a basic factor in providing mathematical models with data to perform spatial analysis of CPSAs.

#### References

- Al-Abed, M., Salhab, J., Ibrahim, H. and Dweri, S. 2018. Quantitative estimation of annual soil loss by integration of remote sensing, GIS and Universal Soil Loss Equation (Case Study: Tartus District, Syria). Annals of Arid Zone 57: 129-134.
- Al-Qutaini 2015. Environmental degradation in Al-Abrash basin. *Master Thesis*, Geographical department, Damascus University.
- Butler, D.M., Franklin, D.H., Ranells, N.N., Poore, M.H. and Green, J.T. 2006. Ground cover impacts on sediment and phosphorus export from manured riparian pasture. *Journal of Environment Quality* 35(6): 2178-2185.
- Chang, K. and Tsai, B. 1991. The effect of DEM resolution on slope and aspect mapping. *Cartography and GIS* 18(1): 69-77.
- Chang, N.B. 2010. Hydrological connections between low-impact development, watershed best management practices, and sustainable development. *Journal of Hydrologic Engineering* 15(6): 384-385.
- Dobos, E., Daroussin, J. and Montanarella, L. 2007. A quantitative procedure for building physiographic units for the European SOTER database. In *Digital Terrain Modeling*. Development and Applications in a Policy Support Environment, European Commission, Springer. pp. 227–259.
- Freund, R.J. and Littell, R.C. 2000. SAS System for Regression. 3<sup>rd</sup> Ed., SAS Institute Inc., Cary, NC, USA.
- Ghebremichael, L.T., Veith, T.L. and Hamlett, J.M. 2013. Integrated watershed-and farm-scale modeling framework for targeting critical source areas while maintaining farm economic viability. *Journal of Environmental Management* 114: 381-394.
- Hahn, C., Prasuhn, V., Stamm, C., Milledge, D.G. and Schulin, R. 2014. A comparison of three simple approaches to identify critical areas for runoff and dissolved reactive phosphorus losses. *Hydrology and Earth System Sciences* 18(8): 2975-2991.
- Ibraheem, H.M., Edriss, Y. and Al-Shater, M.S. 2019. Estimation of runoff depth using GIS maps and soil conservation service –curve number method

- in Al-Abrash basin in Syria. *Annals of Arid Zone* 58(3&4), 117-125.
- Kahiluoto, H., Kuisma, M., Ketoja, E., Salo, T. and Heikkinen, J. 2015. Phosphorus in manure and sewage sludge more recyclable than in soluble inorganic fertilizer. *Environmental Science and Technology* 49(4): 2115–2122.
- Liu, R., Wang, J., Shi, J., Chen, Y., Sun, C., Zhang, P. and Shen, Z. 2014. Runoff characteristics and nutrient loss mechanism from plain farmland under simulated rainfall conditions. *Science of the Total Environment* 468: 1069-1077.
- Lou, H., Yang, S., Zhao, C., Shi, L., Wu, L., Wang, Y. and Wang, Z. 2016. Detecting and analyzing soil phosphorus loss associated with criticalsource areas using a remote sensing approach. *Science of the Total Environment* 573: 397-408.
- Lou, H., Yang, S., Zhao, C., Zhou, Q., Bai, J., Hao, F. and Wu, L. 2015. Phosphorus risk in an intensive agricultural area in a mid-high latitude region of China. *Catena* 127: 46-55.
- Mazahreh, S., Alkharabsheh, M., Bsoul, M., Abu Hammor, D. and Al Mahasneh, L. 2018. Identification and mapping of hot spot areas susceptible to soil erosion in Erak AL KARAK area using geoinformatics. *International Journal* of Research-Granthaalayah 6(6): 246-259.
- McDowell, R.W. 2012. Minimizing phosphorus losses from the soil matrix. *Current Opinion in Biotechnology* 23(6): 860-865.
- Oyama, Y., Matsushita, B. and Fukushima, T. 2015. Distinguishing surface cyanobacterial blooms and aquatic macrophytes using Landsat/TM and ETM+ shortwave infrared bands. *Remote Sensing of Environment* 157: 35-47.
- Peucker, T.K. and Douglas, D.H. 1974. Detection of surface specific points by local parallel processing of discrete terrain elevation data. *Computer Graphics and Image Processing* 4: 375-387.
- Ponce, V.M. and Hawkins, R.H. 1996. Runoff curve number: has it reached maturity. *Journal of Hydrology Engineering* 1: 11-19.
- Renard, K.G., Foster, G.R., Weesies, G.A. and Porter, J.P. 1991. RUSLE: Revised universal soil loss equation. *Journal of Soil Water Conservation* 46(1): 30-33.
- Rivero, R.G., Grunwald, S., Binford, M.W. and Osborne, T.Z. 2009. Integrating spectral indices into prediction models of soil phosphorus in a subtropical wetland. *Remote Sensing of Environment* 113(11): 2389-2402.
- Roszkowska, W. 2013. Rank ordering criteria weighting methods A comparative overview. *Optimum Studia Ekonomiczne NR* 5(65): 14-33.
- Soil Conservation Service (SCS) 1985. Hydrology, National Engineering Handbook. Supplement A,

- Section 4, Chapter 10, Soil Conservation Service, U.S.D.A., Washington, DC.
- Sharpley, A.N. and Jarvie, H.P. 2012. Agriculture management water quality and ecology putting practice into policy. *National Agricultural Biotechnology Council Conference Proceedings* 24: 87-116.
- Shi, L., Liu, P., Kloog, I., Lee, M., Kosheleva, A. and Schwartz, J. 2016. Estimating daily air temperature across the Southeastern United States using high-resolution satellite data: A statistical modeling study. *Environment Research* 146: 51-58.
- Wang, L., Liang, T., Kleinman, P.J. and Cao, H. 2011b. An experimental study on using rare earth elements to trace phosphorous losses from nonpoint sources. *Chemosphere* 85(6): 1075-1079.
- Wang, X., Wang, Q., Yang, S., Zheng, D., Wu, C. and Mannaerts, C.M. 2011a. Evaluating nitrogen removal by vegetation uptake using satellite image time series in riparian catchments. *Science of the Total Environment* 409(13): 2567-2576.
- Wischmeier, W.H. and Smith, D.D. 1978. Predicting rainfall erosion losses: A guide to conservation

- planning. Agriculture Handbook No. 537. USDA/Science and Education Administration, US. Govt. Printing Office, Washington, DC. 58 p.
- Withers, P.J., Sylvester-Bradley, R., Jones, D.L., Healey, J.R. and Talboys, P.J. 2014. Feed the crop not the soil: rethinking phosphorus management in the food chain. *Environmental Science & Technology* 48(12): 6523-6530.
- Xie, W. and Zhao, D. 2016. Controlling phosphate releasing from poultry litter using stabilized Fe-Mn binary oxide nanoparticles. *Science of the Total Environment* 542: 1020-1029.
- Yaghi, H. and Salim, H. 2017. Integration of RS/GIS for surface water pollution risk modeling. Case study: AL-Abrash Syrian coastal basin. International Archives of the Photogrammetry, Remote Sensing and Spatial Information Sciences, Volume XLII-2/W7, 949-954.
- Zhou, H. and Gao, C. 2011. Assessing the risk of phosphorus loss and identifying critical source areas in the Chaohu Lake watershed, China. *Environmental Management* 48(5): 1033-1043.

Printed in June 2020